Int. J. Electrochem. Sci., 15 **(2020)** 4352 – 4367, doi: 10.20964/2020.05.16

International Journal of
ELECTROCHEMICAL
SCIENCE
www.electrochemsci.org

Preparation of a PbO_2 Electrode with Graphene Interlayer and for Electrochemical Oxidation of Doxycycline

Xu Cong[1], *Jiqing Bao*[1,2*]

[1] School of Environmental and Safety Engineering, Changzhou University, Changzhou 213100, China
[2] College of Biological, Chemical Science and Engineering, Jiaxing University, Jiaxing 314001, China
[*]E-mail: baojiqing997441@126.com

Received: 23 November 2019 / *Accepted:* 24 January 2020 / *Published:* 10 April 2020

A graphene interlayer was introduced into a Ti/SnO_2-Sb_2O_3/PbO_2 electrode by electrophoretic deposition and electro position methods to form a Ti/SnO_2-Sb_2O_3/graphene/PbO_2 electrode (G/PbO_2). In comparison to the Ti/SnO_2-Sb_2O_3/PbO_2 electrode (PbO_2), the surface of the G/PbO_2 electrode was flat with fewer surface cracks, and smaller crystal sizes. Cyclic voltammetry (CV) and electrochemical impedance spectroscopy (EIS) results showed that the G/PbO_2 electrode had a large electrochemically active surface area and more active sites. The accelerated lifetime of the G/PbO_2 electrode was 72 h, which was longer than that of the PbO_2 electrode (40 h). In addition, the graphene interlayer improved the ability to generate $OH^{\bullet}$. The real electrochemical oxidation abilities of the G/PbO_2 and PbO_2 electrodes were also studied using doxycycline (DC) as a model pollutant. After 150 min of electrolysis, the DC, total organic carbon (TOC) removal rate and instantaneous current efficiency (ICE) of the G/PbO_2 electrode were 98.5%, 32.3% and 1.80%, respectively, which was higher than those of the PbO_2 electrode (93.6%, 28.7% and 1.60%, respectively). Furthermore, six intermediate products were identified based on HPLC-MS, and oxidation pathways were proposed.

Keywords: graphene; PbO_2 electrode; doxycycline; electrochemical oxidation

1. INTRODUCTION

Antibiotics have been widely used in animal husbandry and for medical treatment because they can inhibit or kill many bacteria [1, 2]. However, most of these antibiotics are not fully utilized and are discharged into bodies of water in the form of prototypes or as metabolites through urine, feces and other ways [3, 4]. Because they cannot be completely absorbed by animals and human beings, these antibiotics have been considered pseudo persistent organic compounds due to their degradation resistance [5]. The continuous and wide use of antibiotics has a great impact on water environments. For example, several antibiotics have been detected in groundwater [6], surface water [7-9] and drinking water [10, 11] in many parts of the world. The existence of these compounds not only enhances the antibiotic resistance

of bacteria but also threatens human health [3, 12]. Therefore, how to effectively remove antibiotics is currently a focus of research.

Doxycycline, as a semisynthetic tetracycline antibiotic, is utilized to prevent and treat gram-positive and gram-negative bacterial infections. The long-term persistence of doxycycline in water is harmful to aquatic ecosystems and human health. Traditional biological and physical methods cannot effectively remove doxycycline from water due to the nature of its molecular structure [6]. Electrochemical advanced oxidation processes (EAOPs) can produce hydroxyl radicals with high oxidation potential (E^0 = 2.8 V) for doxycycline degradation without needing additional oxidants. Due to their simple operation and environmental friendliness, this method has attracted great attention, but the electrochemical oxidation efficiency is highly dependent on the electrode materials [6]. Various materials, such as RuO_2 [6], IrO_2 [13], boron-doped diamond (BDD) [14], and PbO_2 [11], have been used as electrode materials for antibiotic removal [15]. Among them, RuO_2 and IrO_2 can effectively remove antibiotics, but their removal rates of COD and TOC are low, additionally, they are expensive owing to the presence of precious metals [16]. BDD electrodes can effectively remove antibiotics, COD and TOC, but their high price and complicated manufacturing process limit their large-scale application in industry [17]. In contrast, a PbO_2 electrode with a low cost, good conductivity, stable performance, and high oxygen evolution potential has been considered one of the best materials. In previous research, various efforts have been made to improve the stability and performance of PbO_2-based electrodes, including metal element doping (Al [18], La [11], Co and Bi [19]), forming composites (carbon nanotubes [20]), adding intermediate layers (SnO_2-Sb_2O_3 [21] and α-PbO_2 [22]), etc.

Graphene is a two-dimensional carbon nanomaterial that has been widely applied as an additive in anode materials due to having excellent electrical conductivity while also having a high surface area (2630 $m^2 \cdot g^{-1}$) and an effective resistance to reduction [23]. Li et al. [6] reported a RuO_2-TiO_2/Nano-graphene anode for electrochemical degradation of ceftriaxone sodium. In comparison to RuO_2-TiO_2, TiO_2/Nano-G and Nano-G, RuO_2-TiO_2/Nano-graphene showed a higher specific surface area and an improved electrochemical oxidation performance, where the removal rate of ceftriaxone was increased from 76.6% to 90.3% within 100 min. Information regarding a graphene interlayer in a PbO_2 electrode is limited, and it is possible to improve the electrochemical performance and stability of the PbO_2 electrode by adding a graphene interlayer.

In this study, we attempt to introduce a graphene interlayer into a Ti/SnO_2-Sb_2O_3/PbO_2 electrode to form a Ti/SnO_2-Sb_2O_3/graphene/PbO_2 electrode (named G/PbO_2). Scanning electron microscopy (SEM), X-ray diffraction (XRD), cyclic voltammetry (CV), electrochemical impedance spectroscopy (EIS) and accelerated service life tests were used to clarify the effect of the graphene interlayer on the surface morphology, structure, electrochemical performance and stability of the fabricated PbO_2 electrode. In addition, the fabricated electrode was applied to electrochemical oxidation of doxycycline.

2. MATERIALS AND METHODS

2.1 Chemicals

Doxycycline, $Pb(NO_3)_2$, NaF, HNO_3, $SnCl_4 \cdot 5H_2O$, $SbCl_3$, sodium dodecylbenzene sulfonate and Na_2SO_4 were purchased from Sinopharm Chemical Reagent Co., Ltd., China. Graphene was purchased

from Chengdu Organic Chemistry Co., Ltd., Chinese Academy of Sciences, China. All solutions were prepared with deionized water.

2.2 Electrode preparation and characterization

A Ti substrate (TA2, 10 ×10 × 1 mm) was first etched by 10% oxalic acid for 2 h at 80°C to remove the oxide layer on the surface. After pretreatment, the bottom layer of SnO_2-Sb_2O_3 was prepared by a thermal deposition method. A 10 mL mixed solution of isopropanol and hydrochloric acid (isopropanol:HCl = 9:1, v/v) containing 2 g $SnCl_4 \cdot 5H_2O$ and 0.2 g $SbCl_3$ was used as the coating solution. The Ti substrate was coated with the prepared coating solution using a dip-coating method. After that, the Ti substrates were dried at 120°C for 10 min in an oven and then sintered at 500°C for 15 min in a muffle furnace. The above operations were repeated 8 times, and the last sintering time was 1 h. The graphene interlayer was fabricated by using an electrophoretic deposition method. An aqueous solution, to use for deposition, contained 0.5 $g \cdot L^{-1}$ graphene and 0.05 $g \cdot L^{-1}$ sodium dodecylbenzene sulfonate and was first ultrasonically vibrated for 0.5 h. Graphene was then electrophoretic deposited onto the Ti/SnO_2-Sb_2O_3 electrode at 30 V for 20 min in a 100 mL beaker, where a Ti plate, with the same dimensions as above, was used as the cathode. The distance between the anode and cathode was 2 cm. After electrophoretic deposition, the sample was dried at 120°C for 20 min. Then, the PbO_2 layer was electrodeposited onto the obtained electrode at 65°C and 15 $mA \cdot cm^{-2}$ by using a solution consisting of 0.5 M $Pb(NO_3)_2$, 0.1 M HNO_3 and 0.1 $g \cdot L^{-1}$ NaF. The electrode with the graphene interlayer was denoted as G/PbO_2, while the electrode without the graphene interlayer, which was prepared by the same method, was denoted as PbO_2.

Surface morphologies and elemental contents of the fabricated electrodes were characterized by an S-4800 scanning electron microscope (Hitachi, Japan) equipped with an EX-250 energy-dispersive X-ray spectroscopy (Horiba, Japan). The crystal structures of the fabricated electrodes were determined using an XRD-7000 X-ray diffractometer (Shimadzu, Japan) using Cu-Kα radiation as an X-ray source.

The electrochemical performance of the fabricated electrodes was characterized using a series of electrochemical tests, which included cyclic voltammetry (CV) and electrochemical impedance spectroscopy (EIS). The above analyses were performed using a CHI660E electrochemical workstation (Chenhua, China) with a three-electrode setup. The fabricated PbO_2 electrodes, a saturated calomel electrode (SCE), and a Pt wire were used as the working, counter and reference electrodes, respectively.

The accelerated lifetime of the fabricated electrodes was tested using 2 M H_2SO_4 at a current density of 1 $A \cdot cm^{-2}$ and a temperature of 65°C. When the cell voltage rapidly increased above 5 V from the initial value as time increased, it was regarded as anode failure, and the accelerated lifetime was obtained. The actual service lifetime of the electrodes was calculated by Eq. 1 [24]:

$$t_1 = t_2 (\frac{i_2}{i_1})^2 \quad (1)$$

where i_1 and i_2 are the applied current density and accelerated current density, respectively, and t_1 and t_2 are the actual service lifetime and accelerated lifetime, respectively.

The amount of $OH^{\bullet}$ radicals produced during the electrochemical oxidation experiment was measured by fluorescence spectrometry using terephthalic acid as the fluorescence probe. The production of $OH^{\bullet}$ was measured with a current density of 30 $mA \cdot cm^{-2}$, and the fabricated PbO_2 electrodes and Ti plates of the same size were used as the anode and cathode, respectively. One hundred milliliters of an aqueous solution containing 0.5 mM terephthalic acid, 0.25 M Na_2SO_4 and 0.4 $g \cdot L^{-1}$ NaOH was used as the electrolyte. During the experiment, samples were drawn every 5 min and diluted 10 times with deionized water; then, they were analyzed by an F-7000 fluorescence spectrophotometer (Hitachi, Japan). Fluorescence spectra were obtained using an excitation wavelength of 315 nm and recorded in a range of 370-520 nm.

2.3 Electrochemical oxidation of doxycycline

Electrochemical oxidation of doxycycline was carried out in a 100 mL beaker, which contained 50 $mg \cdot L^{-1}$ DC and 0.1 M Na_2SO_4 as a supporting electrolyte, at a temperature of 25℃ and with magnetic stirring. The fabricated PbO_2 electrode and Ti plate were used as the anode and cathode, respectively. The applied current density was 50 $mA \cdot cm^{-2}$, and the distance between the two electrodes was 2 cm.

2.4 analysis

Doxycycline content was detected by ultraviolet spectroscopy at a wavelength of 370 nm (Agilent Cary 60 UV-vis) [25]. The intermediate products were analyzed by HPLC-MS (LCT premier XE, Waters, USA). A Liqui II TOC analyzer was used to measure the TOC change during the experiment. The instantaneous current efficiency (ICE) at each time point was calculated by Eq. 2:

$$ICE = \frac{2.67(TOC_0 - TOC_t) \times F \times V}{8It \times 1000} \quad (2)$$

where TOC_0 and TOC_t are the total organic carbon ($g \cdot L^{-1}$) at time 0 and t (s), respectively, F is the Faraday constant (96478 $C \cdot mol^{-1}$), V is the solution volume (L), and I is the current (A).

3. RESULTS AND DISCUSSION

3.1 Characterization of the electrode surface morphologies

As shown in Figures. 1a and 1b, the surface of the SbO_2-Sb_2O_3 bottom layer had irregular crystal grains that were coarse and dispersed and presented a cauliflower-like morphology. However, under the action of an electric field, graphene was stacked on the bottom layer of SbO_2-Sb_2O_3, and the surface of the electrode became rough and wrinkled. This phenomenon was observed in other literature, for instance, electrophoretic deposition of graphene on a steel mesh [26]. EDS was used to measure the elemental content in the different electrodes. Figures. 1c and 1d show the EDS spectra of the Ti/SnO_2-Sb_2O_3 and Ti/SnO_2-Sb_2O_3/graphene electrodes. As shown in Table 1, after electrophoresis of the graphene interlayer, the C content increased from 1.66% to 34.34% (C peak of Ti/SnO_2-Sb_2O_3 electrode

comes from the conductive adhesive), concluding that graphene covered the Ti/SnO_2-Sb_2O_3 bottom layer. Furthermore, Ti, Sn, and Sb elements were also found in Ti/SnO_2-Sb_2O_3/graphene because X-rays penetrated the graphene interlayer and reached the bottom layer of SbO_2-Sb_2O_3.

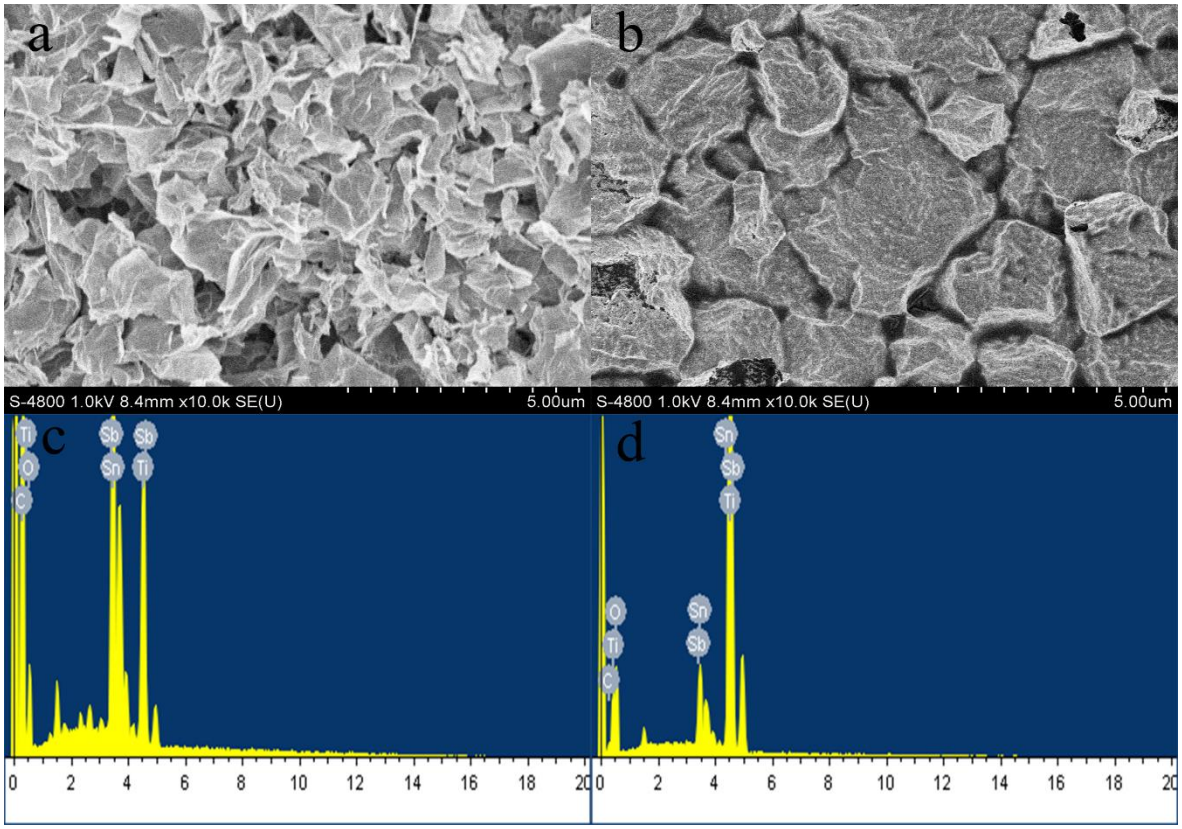

Figure 1. SEM morphologies of (a) Ti/SnO_2-Sb_2O_3/graphene and (b) Ti/SnO_2-Sb_2O_3; EDS spectra of (c) Ti/SnO_2-Sb_2O_3/graphene and (d) Ti/SnO_2-Sb_2O_3.

Table 1. Elemental content analysis of the different electrodes, as calculated from the EDS results

	Ti/SnO_2-Sb_2O_3/graphene		Ti/SnO_2--Sb_2O_3	
Element	wt%	at%	wt%	at%
C	34.34	61.60	1.66	3.95
O	37.37	30.13	34.69	58.44
Ti	18.02	5.86	40.12	31.47
Sn	9.26	2.23	21.90	5.76
Sb	1.01	0.18	1.64	0.38

Figures. 2a and 2b show the SEM morphologies of the G/PbO_2 and PbO_2 electrodes. It is clear found that the surface of the PbO_2 electrode was rough with many cracks (Figure. 2b). However, after the introduction of the graphene interlayer, the electrode surface became smooth, and the number of cracks was greatly reduced (Figure. 2a). The smooth surface of G/PbO_2 can effectively prevent O_2 and electrolyte diffusion into the interior of the electrode, which can improve its stability and prolong its service life.

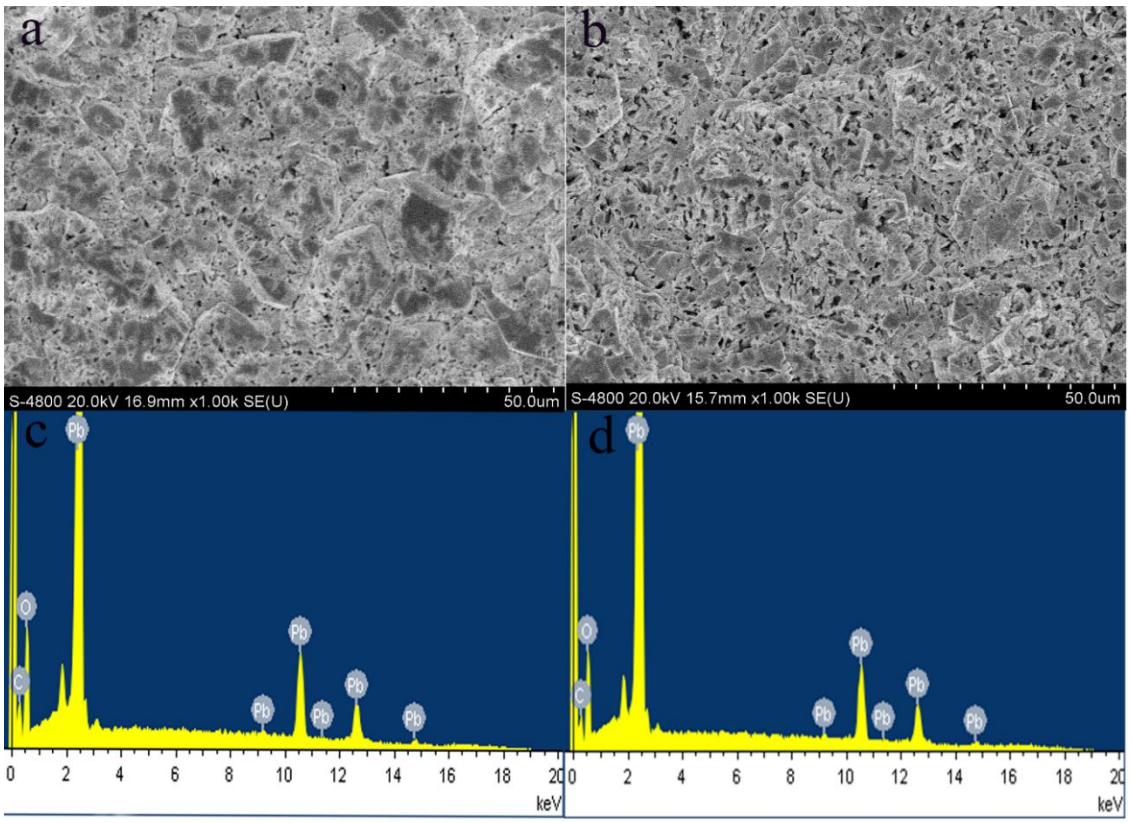

Figure 2. SEM morphologies of (a) G/PbO_2 and (b) PbO_2; EDS spectra of (c) G/PbO_2 and (d) PbO_2.

The smooth surface of G/PbO_2 can be explained by the PbO_2 electrodeposition process [16], as shown in the following formula:

$$H_2O \rightarrow H^+ + e^- + OH^\bullet \quad (3)$$

$$Pb^{2+} + OH^\bullet \rightarrow Pb(OH)^{2+} \quad (4)$$

$$Pb(OH)^{2+} + H_2O \rightarrow Pb(OH)_2^{2+} + H^+ + e^- \quad (5)$$

$$Pb(OH)_2^{2+} \rightarrow PbO_2 + 2H^+ \quad (6)$$

In the initial stage of PbO_2 crystal formation, due to the large specific surface area of graphene, a large amount of $OH^\bullet$ generated from formula (3) was adsorbed on the surface of the graphene interlayer [20, 27]. As a result, more PbO_2 crystal nuclei were formed through formula (3-6), while the growth of crystal nuclei was inhibited, thus leading to a smooth PbO_2 layer [20]. With an extended electrodeposition time, there was no significant difference between the carbon content of G/PbO_2 and PbO_2 (Table 2), indicating that the graphene interlayer was completely covered by PbO_2 crystals (C peak comes from the conductive adhesive).

Table 2. Elemental content analysis of the different electrodes, as calculated from the EDS results

	G/PbO_2		PbO_2	
Element	wt%	at%	wt%	at%
C	6.44	25.60	6.45	25.59
O	17.30	55.42	19.24	57.32
Pb	76.72	18.98	74.31	17.10

The influence of the graphene interlayer on the structure of the PbO_2 electrode was studied by XRD. Figure. 3 shows the XRD patterns of PbO_2 and G/PbO_2. The main diffraction peaks observed at 2θ=25.4°, 31.9°, 36.7°, 49.0°, 52.1°, 58.8°, 62.4°, and 74.4° can be ascribed to the (110), (101), (200), (211), (220), (310), (301) and (321) planes of β-PbO_2, respectively. This agrees well with the standard data of the JCPDS card (number: 76-0564). In addition, it can be found that the intensity and the half-widths of G/PbO_2 are increased, which means that the degree of crystallization of the PbO_2 crystal increases and the crystal size decreases due to the introduction of the graphene interlayer. The same phenomenon is also observed in other modified electrodes [28]. The average crystal sizes of the G/PbO_2 and PbO_2 electrodes are estimated by the Scherrer equation with the strongest diffraction peak at 2θ = 25.4° [29]. The results are shown in Table 3. The crystal size of the G/PbO_2 is 39.5 nm, which is smaller than the 47.9 nm of PbO_2 and the values of other electrodes [20, 21, 30]. This may be due to the graphene interlayer providing more PbO_2 crystal nuclei, while the growth of the crystals is inhibited, thus decreasing the crystal size. The small crystalline grain means more active sites, which is beneficial for improving the pollutant degradation performance of the electrodes.

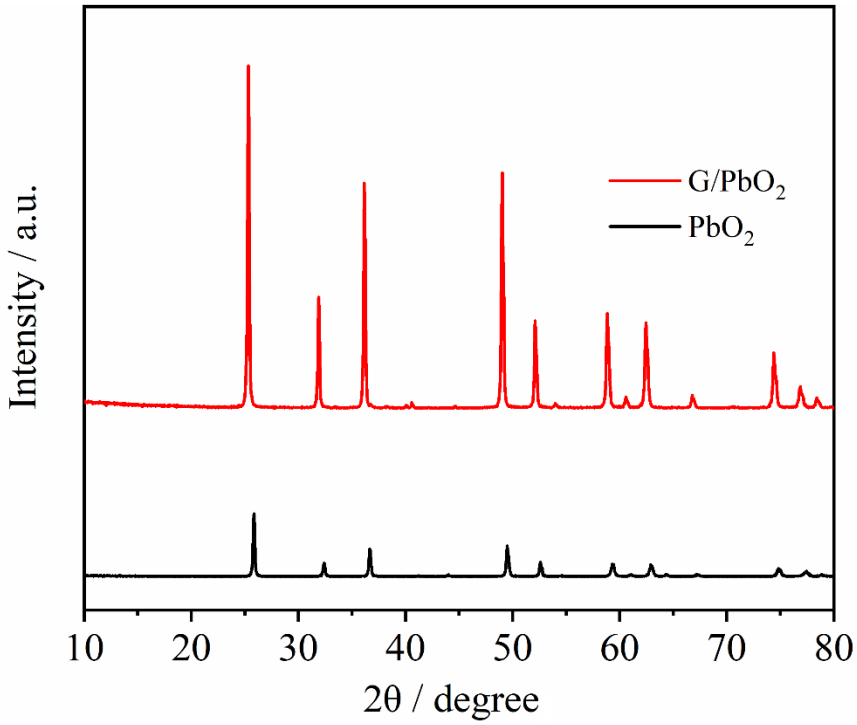

Figure 3. XRD patterns of G/PbO_2 and PbO_2.

Table 3. Crystalline grain diameters of the G/PbO_2 and PbO_2.

Electrode	Half-height width (110 plane)	Average size (nm)
G/PbO_2	0.204	39.5
PbO_2	0.168	47.9

3.2 Electrochemical performance test

The electrochemical performance is related to its electrochemical active surface area and the number of active sites [16, 31], both of which can be indirectly evaluated by voltammetric charge quantity (q*). A large q* indicates a higher electrochemical performance [30]. The q* for our electrodes are evaluated using Eq. 7, as reported in the literature [20, 30]:

$$(q^*)^{-1} = (q_T)^{-1} + kv^{0.5} \quad (7)$$

where q_T is the theoretical electrochemical active surface area, v is the scan rate, and k is a constant. Figures. 4a and 4b show the CV curves of the G/PbO_2 and PbO_2 electrodes performed in a 0.5 M H_2SO_4 solution at a scan rate of 10-50 mV·$s^{-1}$and a potential range of 0-2 V (vs. SCE). q* was calculated by an integration of the CV curves. Figure. 4c shows the relationship between q* and scanning rate. The q* value of G/PbO_2 were larger than those of the PbO_2 electrode, which indicates that the G/PbO_2 electrode had a larger active surface area and more active sites.

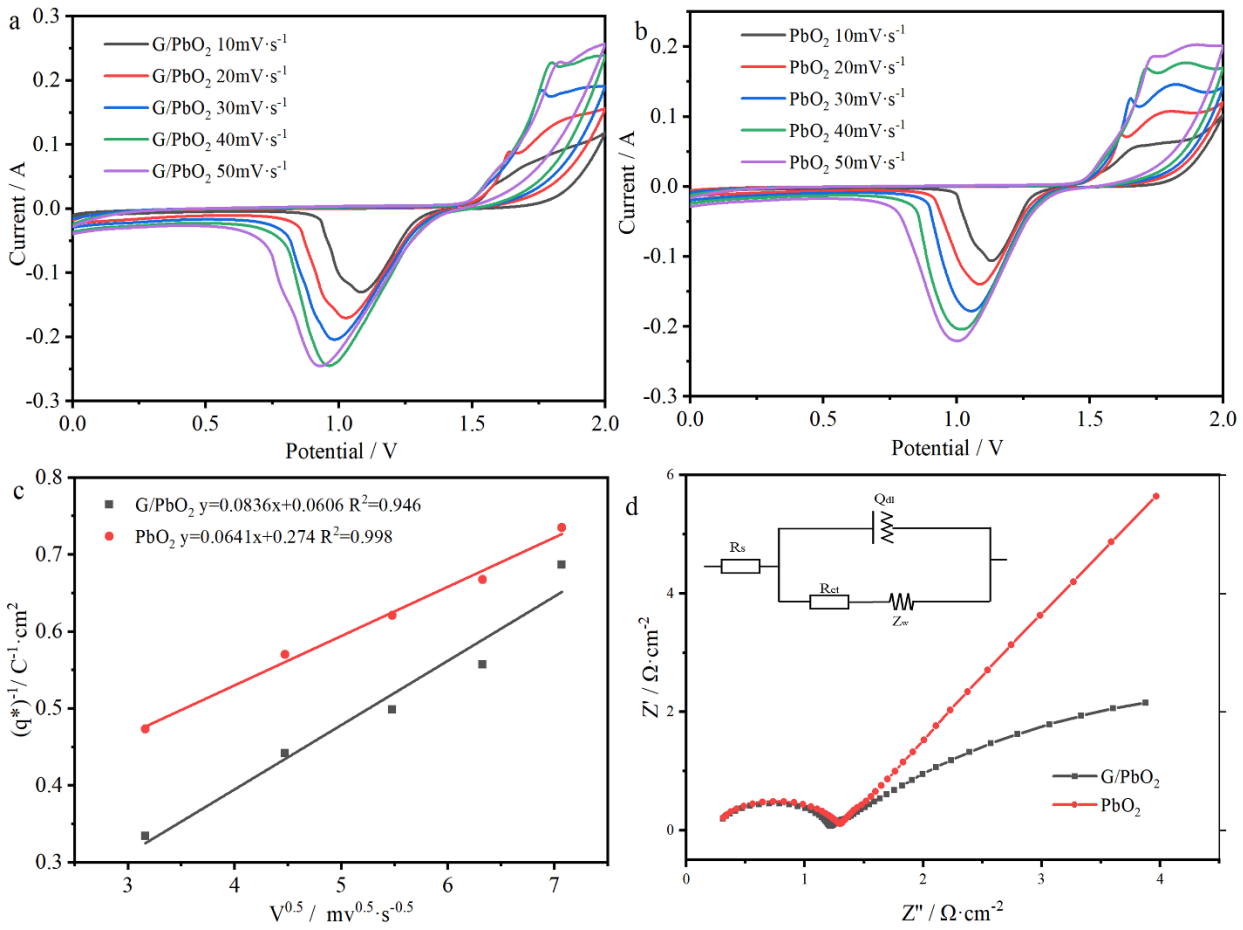

Figure 4. (a) , (b) Cyclic voltammograms of G/PbO_2 and PbO_2 in a 0.5 M H_2SO_4 solution at a scan rate of 10-50 mV·S^{-1} and in a potential range of 0-2 V (vs. SCE); (c) relationship of q* versus the square root of the scan rate; and (d) Nyquist plots of G/PbO_2 and PbO_2 with an equivalent circuit diagram (insert).

EIS was used to further investigate the effect of the graphene interlayer on the electrochemical performance of the electrode. Figure. 4d displays the Nyquist plots obtained for G/PbO_2 and PbO_2 at the open-circuit voltage in a 0.5 M H_2SO_4 solution over a frequency range of 0.1 Hz to 10 kHz with an alternating signal of 5 mV. An equivalent circuit expressed as Rs(Qdl(RctZw)), as shown in the inset of Figure. 4f, was utilized to fit the EIS results, and the values of each circuit component are shown in Table 4. Rs is the solution resistance, Rct is the charge transfer resistance, Qdl is introduced to replace the electric double layer capacitor, and Zw is the solution diffusion into PbO_2. The Rct of the G/PbO_2 electrode was 0.86 $\Omega \cdot cm^{-2}$, which was lower than that of the PbO_2 electrode (1.04 $\Omega \cdot cm^{-2}$) and indicated that G/PbO_2 had faster charge transfer and higher oxygen evolution reaction activity [16, 20]. Based on the reaction mechanism of oxygen evolution on the PbO_2 electrode, the number of active sites determines the oxygen evolution activity of the PbO_2 film. When there are more active sites, the reaction activity of the film is increased [16]. Hence, the low Rct of the G/PbO_2 electrode further illustrated that G/PbO_2 had more active sites. A higher Zw value means a higher resistance of diffusion transmission, which inhibits the electrolyte from reaching the electrode surface and extends the life of the electrode. These results indicated that the introduction of a graphene interlayer can not only enhance the charge transfer but also improve the life of the electrode.

Table 4. Simulated values of each circuit component

Electrode	Rs ($\Omega \cdot cm^{-2}$)	Qdl ($\Omega \cdot cm^{-2}$ S^n)	n	Rct ($\Omega \cdot cm^{-2}$)	Zw (S $s^{0.5}$ $\cdot cm^{-2}$)
G/PbO_2	0.26	1.034	0.97	0.86	12.86
PbO_2	0.25	1.028	0.96	1.04	0.71

Accelerated lifetime is another important factor for evaluating the practical application of electrodes. The accelerated lifetimes of the G/PbO_2 and PbO_2 electrodes were 72 h and 40 h, respectively (Figure. 5). According to Eq. 1, the actual service lifetime of G/PbO_2 was 28800 h, which was 1.8 times that of the PbO_2 electrode and other PbO_2 electrodes, such as 21400 h for porous Ti/SnO_2-Sb_2O_3/PbO_2 [16], 18300 h for Ti/SnO_2-Sb_2O_5/PbO_2-PVDF (1.0 wt%) [32] and 230 h for a Ti/PbO_2 electrode [33]. The above results showed that the graphene interlayer effectively improves the service lifetime. The improved accelerated lifetime can be explained by the small number of cracks and smooth surface of G/PbO_2, which effectively inhibit the electrolyte and O_2 from diffusing to the substrate and forming nonconductive TiO_2.

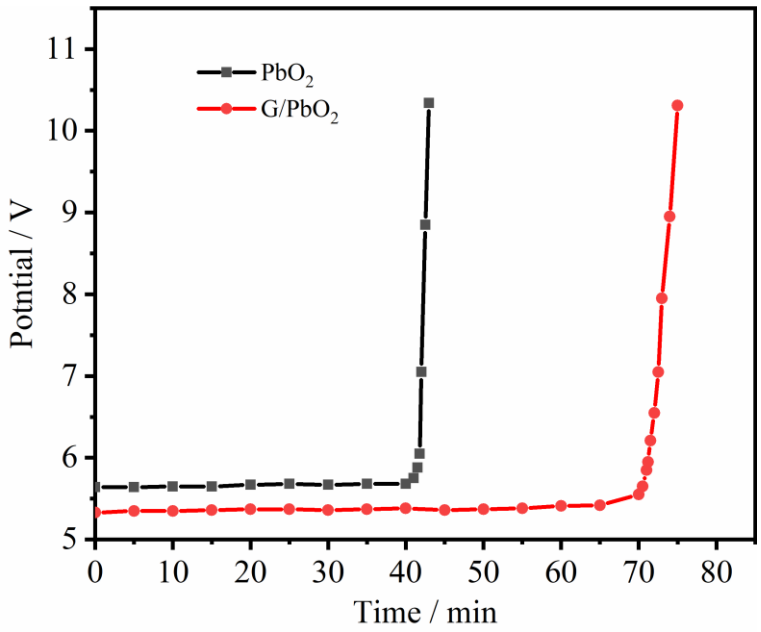

Figure 5. Accelerated lifetime test of the G/PbO_2 and PbO_2.

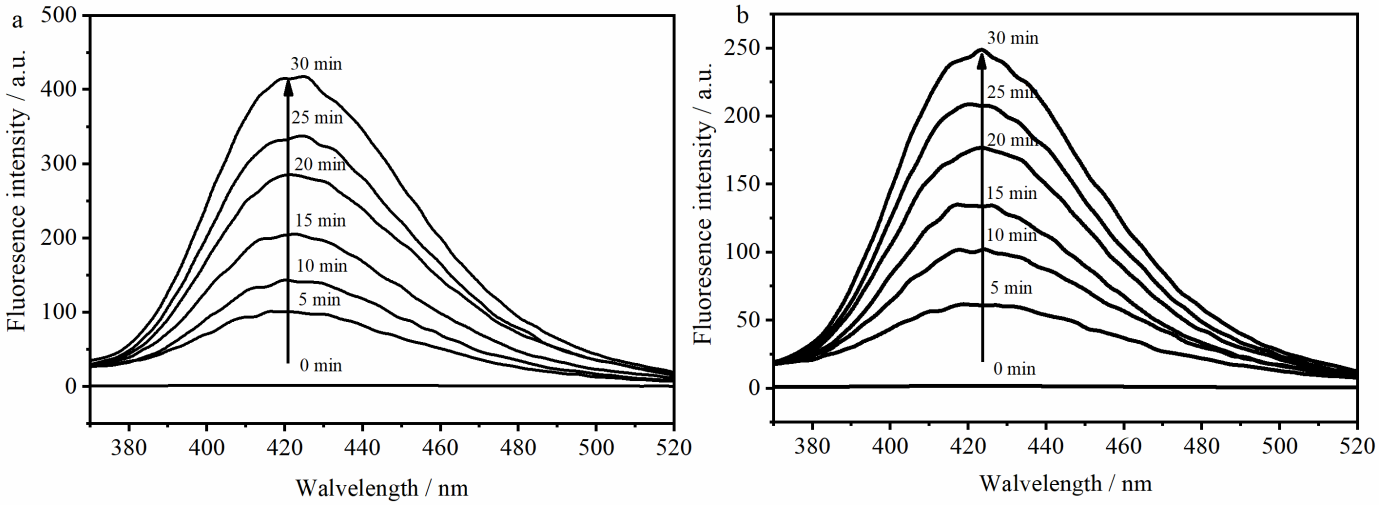

Figure 6. Fluorescence spectra observed during the electrochemical oxidation processes using the (a) G/PbO_2 and (b) PbO_2.

Pollutants are mainly degraded by the ·OH radicals generated in the electrochemical oxidation process using the PbO_2 electrode [20, 33]. Hence, the ability to generate $OH^{\bullet}$ can more accurately reflect the electrochemical properties of the electrode materials. Terephthalic acid as a ·OH radical scavenger can react with ·OH radicals to produce 2-hydroxyterephthalic acid with high fluorescence, and the fluorescence intensity of 2-hydroxyterephthalic acid is approximately equal to the number of generated $OH^{\bullet}$ radicals. As shown in Figure. 6, the fluorescence intensity of 2-hydroxyterephthalic acid at 425 nm for the fabricated electrode increased with increasing electrolysis time, indicating that ·OH radicals were constantly generated in the electrochemical oxidation process. Comparing the fluorescence intensity of

G/PbO_2 and PbO_2, it is found that the fluorescence density was higher than that of PbO_2, which indicated that G/PbO_2 had higher electrocatalytic activity and could oxidize pollutants more effectively. This may be due to its smaller crystal size and larger active surface area, thus providing more active sites for the generation of $OH^{\bullet}$ radicals.

3.3 Electrochemical oxidation of doxycycline

3.3.1 Cyclic voltammetry analyses

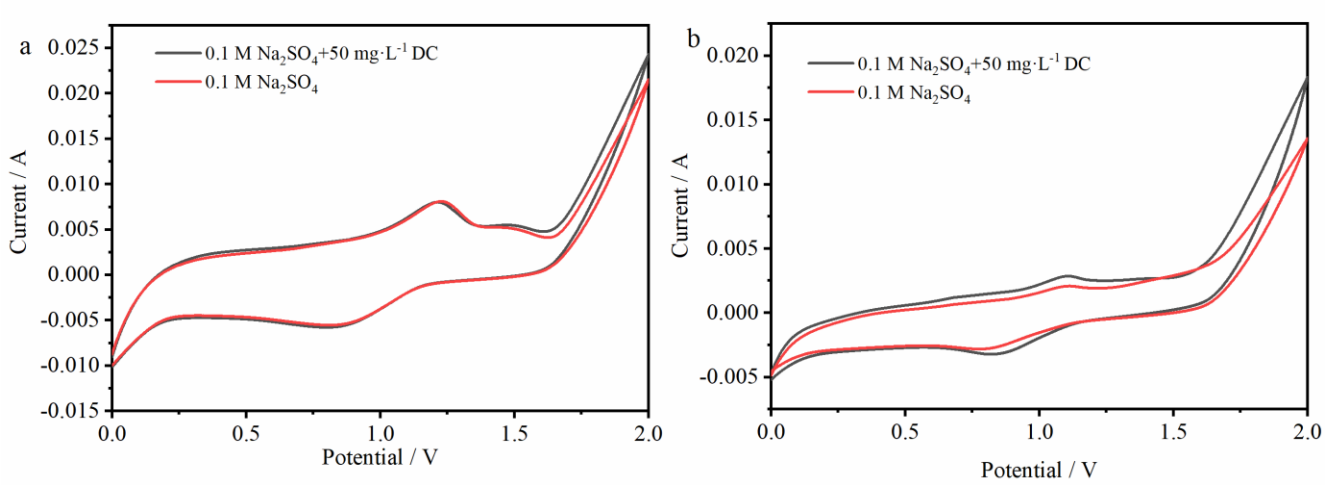

Figure 7. Cyclic voltammetry curves of the different electrodes: (a) G/PbO_2, (b) PbO_2 in 0.1 M Na_2SO_4 and 0.1 M Na_2SO_4 + 50 mg·L^{-1} DC.

The electrochemical characteristics of DC oxidation with the G/PbO_2 and PbO_2 electrodes were investigated by using cyclic voltammetry. As shown in Figure. 7, after 50 mg·L^{-1} DC was added, no additional oxidation peaks were found in the CV curves of both G/PbO_2 and PbO_2. Therefore, doxycycline was indirectly oxidized by hydroxyl radicals generated by the electrochemical oxidation in this experiment.

3.3.2 Doxycycline oxidation experiments.

To further evaluate the effect of the graphene interlayer on electrode performance, experiments on the electrochemical oxidation of doxycycline were carried out using the fabricated electrodes. After 150 min, the removal rate of doxycycline by G/PbO_2 was 98.5%, while that of PbO_2 was only 93.6% (Figure. 8a).

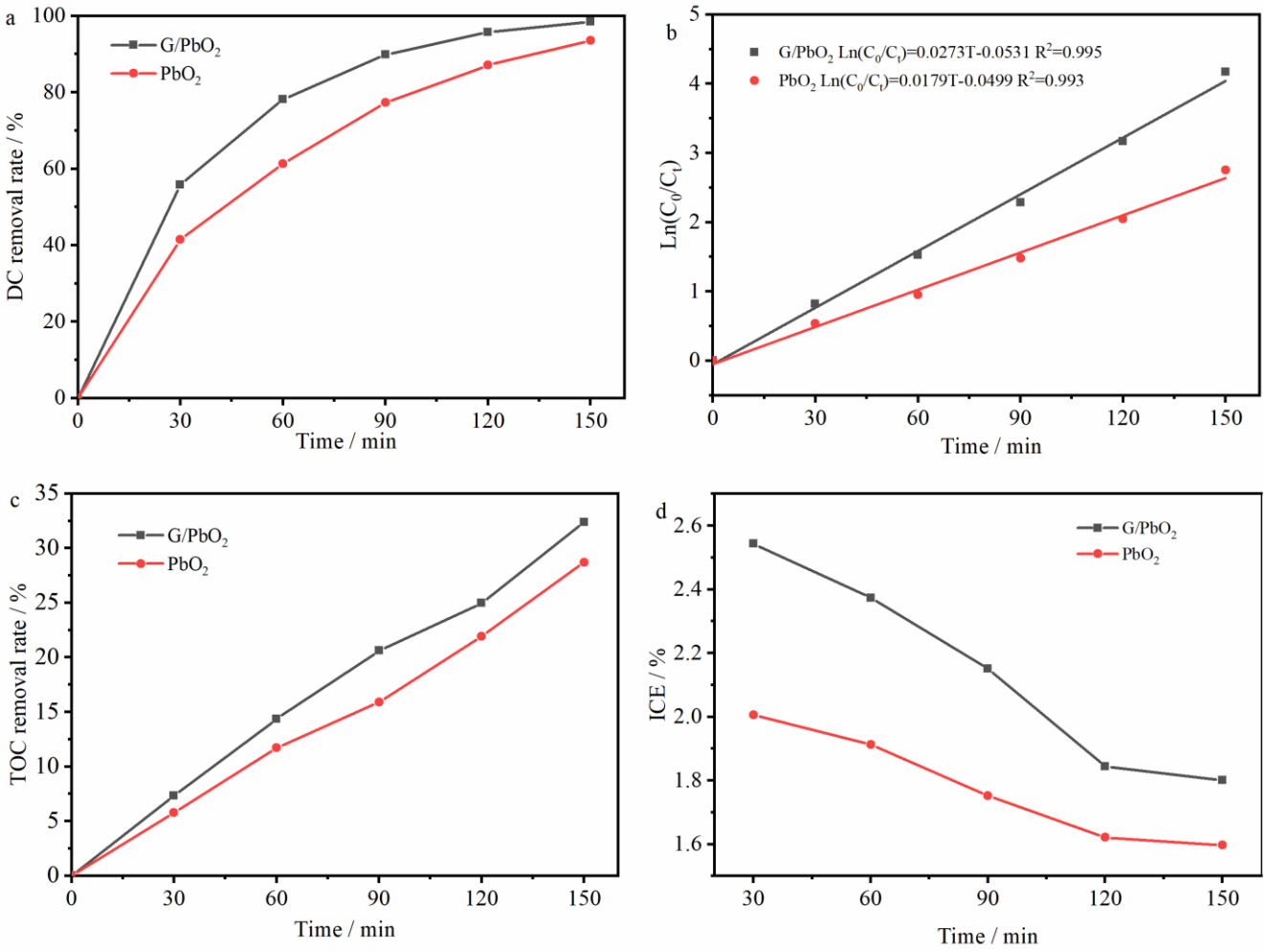

Figure 8. (a) Doxycycline removal rate, (b) kinetic analysis curves, (c) TOC removal rate, and (d) ICE of G/PbO_2 and PbO_2 at different times (experimental conditions: 0.1 M Na_2SO_4, current density of 50 $mA \cdot cm^{-2}$, and initial DC concentration of 50 $mg \cdot L^{-1}$).

In addition, as shown in Figure. 8b, it is found that the oxidation of DC on the G/PbO_2 and PbO_2 electrodes followed pseudo-first-order kinetics, as shown in Eq. 8:

$$Ln(C_0/C_t) = kt \quad (8)$$

where C_0 is the initial DC concentration ($mg \cdot L^{-1}$), C_t ($mg \cdot L^{-1}$) is the DC concentration at time t (min), and k (min^{-1}) is the pseudo-first-order rate constant. The reaction rate constant (k) of G/PbO_2 was 0.0273 min^{-1}, which is 1.53 times greater than that of PbO_2 (0.0179 min^{-1}). This indicated that DC could be oxidized more rapidly with the G/PbO_2 electrode.

The reduction of TOC during the experiment can reflect the mineralization ability of the electrode to the pollutant. As shown in Figure. 8c, the TOC removal rate of G/PbO_2 was 32.3% within 150 min, faster than the 28.7% with the PbO_2 electrode. In addition, the ICE was calculated according to the obtained TOC value (Figure. 8d). The ICE values of G/PbO_2 and PbO_2 were 1.80% and 1.60%, respectively, indicating that G/PbO_2 had a higher doxycycline degradation efficiency with a lower energy consumption than the PbO_2 electrode. In addition, Table 5 shows the DC removal efficiencies studied by other scholars and the experimental results of this work. Compared with this work, Ti/IrO_2 is

expensive and has poor degradation efficiency. Fenton oxidation displayed excellent degradation efficiency. However, it needs additional H_2O_2 and Fe^{2+} and requires acidic conditions and complex operations, which limits its large-scale application. Photocatalyst degradation shows worse removal efficiency with a long processing time and requires an extra auxiliary light source. As a result, the G/PbO_2 electrode is more suitable for DC removal.

Table 5. Comparisons of the removal efficiencies in this work and other relevant research

Method	Material	Condition	Reaction time (min)	Removal rate	Ref
Electrochemical oxidation	G/PbO_2	Applied current density: 50 mA·cm^{-2}, volume:100 mL, electrode size: 1 cm × 1 cm, DC concentration: 50 mg·L^{-1}	150	98.5%	this work
Electrochemical degradation	Ti/IrO_2	Applied current density: 1.5 A, volume: 500 mL, electrode size: 150 mm × 50 mm, DC concentration: 100 mg·L^{-1}	6 h	99.4%	[13]
Heterogeneous Fenton-like	Magnetic Fe_3O_4 chitosan microspheres	Catalysts: 0.1 g, volume: 200 mL, concentration: 50 mg·L^{-1}, H_2O_2: 10 mM, pH=3	120	96.0%	[34]
Fenton oxidation	H_2O_2 and Fe^{2+}	Volume: 200 mL, DC concentration: 100 mg·L^{-1}, Fe^{2+}: 25 mg·L^{-1}, H_2O_2: 611 mg·L^{-1}	120	98.9%	[35]
Photocatalyst degradation	Span60-assisted preparation of $BiOV_4$	Catalysts: 20 mg, volume: 100 mL, DC concentration: 20 mg·L^{-1}, 300 W Xe lamp	120	89.5%	[36]
Photocatalyst degradation	Magnetic polymer-ZnO composite	Catalysis: 0.5 g, volume: 200 mL, DC concentration: 25 mg·L^{-1}, 30 W UV-C lamp	6 h	76.5%	[37]
Photocatalyst degradation	Multiwalled carbon nanotubes (MWCNTs)/a-Bi_2O_3 nanosheets	Catalyst: 50 mg, volume: 50 mL, DC concentration: 10 mg·L^{-1}, 150 W Xe lamp	120	91%	[1]

3.4 Identification of products and degradation pathways

To further elucidate the degradation mechanism of DC and possible reaction pathways, the intermediate products during DC oxidation were determined by HPLC-MS. The main intermediate

products include mass to charge ratios of m/z = 475, 448, 414, 405, 402, 375, 349 and 306, and the proposed degradation mechanism was proposed by combining previous reports, as shown in Figure. 9 [34, 38-41].

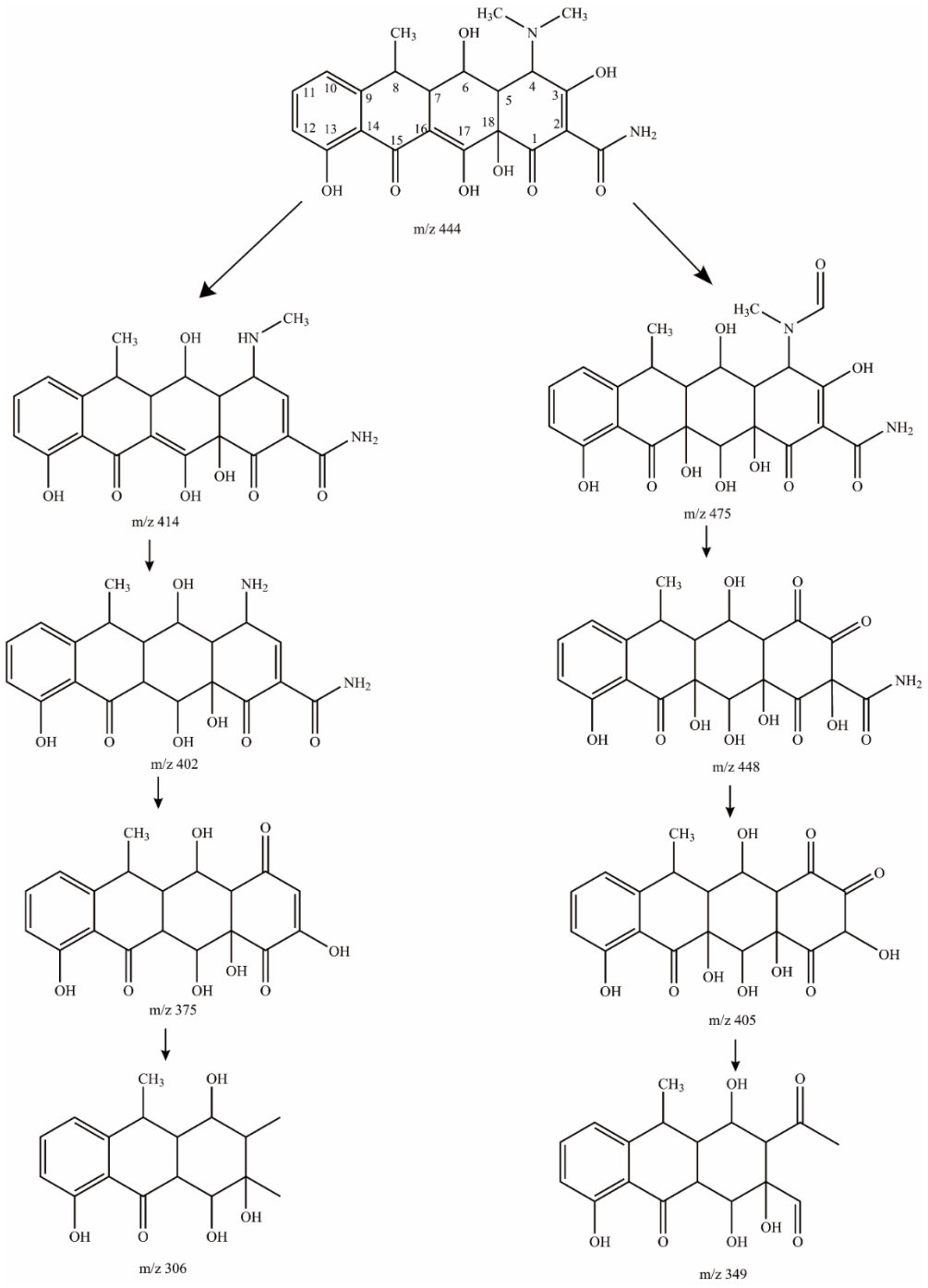

Figure 9. Proposed reaction pathway for the electrochemical oxidation of DC.

Pathway 1: $OH^{\bullet}$ attacked the double bonds at the C2-C3 position, and demethylation reactions caused by oxidation of the amino group form m/z = 414 [41]. Afterward, the acylamido group at the C2 position was replaced by a hydroxyl group. The C=C at C16-C17 was destroyed by $OH^{\bullet}$, and demethylation processes formed m/z = 402. As the continuous proceeding of oxidation, $OH^{\bullet}$

continuously attacked the ester groups at the C1-C2 position, and ring-opening reactions occurred, resulting in the intermediate product of m/z = 306 [40]. Pathway 2: m/z = 475 was due to one methyl of the amino group oxidizing to an aldehyde group, and the C=C at the C16 position was attacked by the hydroxyl radical [34, 38]. Then, $OH^{\bullet}$ attacked the amino group at the C4 position, producing a ketone group, and the C=C at the C16 position forms m/z = 448 [39]. Afterward, $OH^{\bullet}$ attacked the acylamido group at C2 and form m/z = 405. $OH^{\bullet}$ continuously attacked the ester groups at the C1 and C3 positions, and ring-opening reactions occurred, resulting in the intermediate product of m/z = 349. Ultimately, as the electrochemical oxidation process proceeded, the above intermediate products were eventually converted into CO_2 and H_2O, which was inferred by the TOC analysis.

4. CONCLUSION

In this study, we successfully prepared a Ti/SnO_2-Sb_2O_3/PbO_2 electrode (G/PbO_2) with a graphene interlayer by electrophoretic deposition and electro position methods. The obtained G/PbO_2 showed a smoother surface area with fewer cracks and smaller crystal sizes compared to those of the PbO_2 electrode. In addition, the electrochemical performance test results indicated that the G/PbO_2 electrode had a larger voltammetric charge quantity (q*) and a lower charge transfer resistance (Rct). The accelerated lifetime of the G/PbO_2 electrode was 72 h, which was longer than that of the PbO_2 electrode (40 h). In addition, the graphene interlayer could further increase the ability to generate $OH^{\bullet}$. The results of the electrochemical oxidation experiments showed that G/PbO_2 exhibited excellent doxycycline degradation activity. After 150 min of electrolysis, the doxycycline and TOC removal rates as well as the ICE of the G/PbO_2 electrode were 98.5%, 32.3% and 1.80%, respectively, higher than the 93.6%, 28.7% and 1.60% of the PbO_2 electrode. All the results indicated that the graphene interlayer could effectively improve the performance of the PbO_2 electrode. Finally, the possible electrochemical oxidation pathways were proposed based on the six detected intermediate products during the oxidation process.

FUNDING
This research was funded by Zhejiang Province Nature Science Foundation of China (LY18E040002) and the Jiaxing Science and Technology Project (2018AY32040).

ACKNOWLEDGMENTS
We wish to thank anonymous reviewers for their comments, which improved the paper greatly.

References

1. W. Liu, J. Zhou and J. Zhou, *J. Mater. Sci.,* 54 (2018) 3294.
2. A. Mohammad, C. H. Yen, M. Schneider, B. Lowry, F. Yerlikaya, G. Whitesell, B. Leisssa, P. J. Faustino and S. R. Khan, *Anal. Methods.,* 10 (2018) 1842.
3. Y. Liu, C. Wang, Z. Sui and D. Zou, *Sep. Purif. Technol.,* 203 (2018) 29.
4. C. García-Delgado, E. Eymar, R. Camacho-Arévalo, M. Petruccioli, S. Crognale and A. D'Annibale, *J. Chem. Technol. Biotechnol.,* 93 (2018) 3394.
5. D. Chen, B. Li, Q. Pu, X. Chen, G. Wen and Z. Li, *J. Hazard. Mater.,* 373 (2019) 303.

6. D. Li, X. Guo, H. Song, T. Sun and J. Wan, *J. Hazard. Mater.,* 351 (2018) 250.
7. M. A. Aukidy, P. Verlicchi, A. Jelic, M. Petrovic and D. Barcelò, *Sci. Total Environ.,* 438 (2012) 15.
8. N. Gottschall, E. Topp, C. Metcalfe, M. Edwards, M. Payne, S. Kleywegt, P. Russell and D. R. Lapen, *Chemosphere*, 87 (2012) 194.
9. Q.Q. Zhang, G.G. Ying, C.G. Pan, Y.S. Liu, and J.L. Zhao, *Environ. Sci. Technol.,* 49 (2015) 6772.
10. S. Wang, X. Li, H. Zhao, X. Quan, S. Chen and H. Yu, *Water Res.,* 134 (2018) 162.
11. Y. Xia and Q. Dai, *Chemosphere*, 205 (2018) 215.
12. C. Annabi, F. Fourcade, I. Soutrel, F. Geneste, D. Floner, N. Bellakhal and A. Amrane, *J.Environ. Manage.,* 165 (2016) 96.
13. M. Miyata, I. Ihara, G. Yoshid, K. Toyod and K. Umetsu, *Water Sci. Technol.,* 63 (2011) 456.
14. H. B. Ammar, M. B. Brahim, R. Abdelhédi and Y. Samet, *Sep. Purif. Technol.,* 157 (2016) 9.
15. R. Kaur, J. P. Kushwaha and N. Singh, *Chemosphere*, 193 (2017) 685.
16. J. Xing, D. Chen, W. Zhao, X. Peng, Z. Bai, W. Zhang and X. Zhao, *RSC Adv.,* 5 (2015) 53504.
17. D. Zhi, J. Qin, H. Zhou, J. Wang and S. Yang, *J. Appl. Electrochem.,* 47 (2017) 1313.
18. J. Chen, Y. Xia and Q. Dai, *Electrochim. Acta*, 165 (2015) 277.
19. L. Chang, Y. Zhou, X. Duan, W. Liu and D. Xu, *J. Taiwan. Inst. Chem. Eng.,* 45 (2014) 1338.
20. X. Duan, C. Zhao, W. Liu, X. Zhao and L. Chang, *Electrochim. Acta*, 240 (2017) 424.
21. W. Zhao, J. Xing, D. Chen, D. Jin and J. Shen, *J. Electroanal. Chem.,* 775 (2016) 179.
22. H. Lin, J. F. Niu, J.L. Xu, Y. Li and Y.H. Pan, *Electrochim. Acta*, 97 (2013) 167.
23. X.Y. Bao and J.Q. Bao, *J. Electrochem. Soc.,* 165 (2018) H177.
24. Q. Bi, W. Guan, Y. Gao, Y. Cui, S. Ma and J. Xue, *Electrochim. Acta*, 306 (2019) 667.
25. Y. Zhang, J. Shi, Z. Xu, Y. Chen and D. Song, *Chemosphere*, 202 (2018) 661.
26. B. Jaleh, K. Shariati, M. Khosravi, A. Moradi, S. Ghasemi and S. Azizian, *Colloids Surface., A.,* 577 (2019) 323.
27. A.B. Velichenko, R. Amadelli, E.V. Gruzdeva, T.V. Luk'yanenko and F.I. Danilov, *J. Power Sources*, 191 (2009) 103.
28. C.B. Tang, C. Deng, L.H. Yu and J.Q. Xue, *Rare Meta. Mat. Eng.,* 48 (2019) 147.
29. Q. Dai, J. Zhou, X. Meng, D. Feng, C. Wu and J. Chen, *Chem. Eng. J.,* 289 (2016) 239.
30. Q. Dai, Y. Xia and J. Chen, *Electrochim. Acta*, 188 (2016) 871.
31. L. Zhang, L. Xu, J. He and J. Zhang, *Electrochim. Acta*, 117 (2014) 192.
32. Q. Zhuo, Q. Xiang, H. Yi, Z. Zhang, B. Yang, K. Cui, X. Bing, Z. Xu, X. Liang, Q. Guo and R. Yang, *J. Electroanal. Chem.,* 801 (2017) 235.
33. W. Zhao, J. Xing, D. Chen, Z. Bai and Y. Xia, *RSC Adv.,* 5 (2015) 26530.
34. X. Li, K. Cui, Z. Guo, T. Yang, Y. Cao, Y. Xiang, H. Chen and M. Xi, *Chem. Eng. J.,* 379 (2020) 122324.
35. A.A. Borghi, M.F. Silva, S.A. Arni, A. Converti and M.S.A. Palma, *J.Chem.,* 2015 (2015) 1.
36. Y.J. Jiang, W.S. Jiang, D.J. Feng, X.Y. An, X.Y. Lu, W.T. Qiu, and Y. Cai, *Environ. Pollut. Control*, 39 (2017) 170.
37. A. Mohammadi and S. Pourmoslemi, *Water Sci. Technol.,* 2017 (2018) 791.
38. W. Wang, Q. Han, Z. Zhu, L. Zhang, S. Zhong and B. Liu, *Adv. Powder Technol.,* 30 (2019) 1882.
39. J. Wang, D. Zhi, H. Zhou, X. He and D. Zhang, *Water Res.,* 137 (2018) 324.
40. Z. Zhang, Z. Pan, Y. Guo, P. K. Wong, X. Zhou and R. Bai, *Appl. Catal. B.,* 261 (2020) 118212.
41. N. Barhoumi, H. Olvera-Vargas, N. Oturan, D. Huguenot, A. Gadri, S. Ammar, E. Brillas and M. A. Oturan, *Appl. Catal. B.,* 209 (2017) 637.